https://doi.org/10.5194/egusphere-2025-500
Preprint. Discussion started: 1 July 2025

Active Piedmont Zone Deformation, a manifestation of activity on the 'Master Ray Fault'; insight into the seismic hazard analysis of the Tehran metropolitan area

Mohammad R. Ghassemi[a*], Maryam Heydari[b*]

[a] Research Institute for Earth Sciences, Geological Survey of Iran, Azadi Square, Meraj Avenue, P.O. Box 131851494, Iran

[b] Institute of Earth and Environmental Sciences, University of Freiburg, Albertstr. 23b, 79104 Freiburg, Germany

[*] Corresponding authors: ghassemi.m.r@gmail.com

maryam.heydari@geologie.uni-freiburg.de (geochronology)

Abstract

The piedmont zone in the frontal active regions of the orogenic belts exhibits various deformation patterns, which helps unravel the seismic sources for cities that flourish in such tectonic settings. A detailed analysis of the active folding, faulting, and related morphological features of the Quaternary alluvial units disclose prominent thrust faults in the Tehran piedmont zone. These faults are kinematically related and play a vital role in a better understanding of the seismic hazard of the Tehran metropolitan area. The five south-dipping thrust faults, the related hanging-wall folding and subsidiary faulting accommodate a considerable amount of north-south shortening during Quaternary. The shortening is observed in the alluviums and the underlying Eocene volcanic bedrock. Interestingly, in western Tehran, the Chitgar area discloses a type locality for active fault-bend folding, backthrusting, oblique-slip normal faulting and fault inversion in the piedmont zone. Our optically stimulated luminescence dating on the Late Pleistocene alluviums in the Chitgar area constrains the slip rate of the primary and secondary faults. According to our analyses, we introduce the 'Master Ray Fault' as a crucial seismogenic fault of the Tehran region, manifested as south-dipping thrust faults in the piedmont zone. We estimate the minimum slip rate on the Master Ray Fault to be ca. 0.50 mm a^{-1}. Our study offers a crucial methodological framework for improving the existing understanding on Quaternary thrust fault kinematics and associated morphological features, aiding in the unveiling of potential seismic sources in metropolitan areas located in piedmont zones adjacent to active orogenic belts.

Keywords: piedmont deformation, OSL dating, Master Ray Fault, Chitgar Fault, seismic hazard, Tehran

1 Introduction

Forward propagation of deformation fronts in the orogenic systems progressively incorporates the proximal parts of the foreland basin (e.g., Iaffa et al., 2011). The structures in the proximal foreland region can take on different configurations depending on regional and local geometry, deformation history, and rheological characteristics of the foreland terrane. The proximal foreland structures may include compartmentalized piggyback basins or broken foreland (Jordan et al., 1983; DeCelles and Giles, 1996), inherited extensional faults (Iaffa et al., 2011), forebergs

https://doi.org/10.5194/egusphere-2025-500
Preprint. Discussion started: 1 July 2025

(Florensov and Solonenko, 1963), pop-ups (von Hagke et al., 2024), backthrusts and triangle zones (McMechan, 2023, von Hagke et al., 2024), and shortcut thrusts (Coward, 1994).

A drastic change in the deformed materials (bedrock *vs* alluvium) and structural geometry (thick-skinned *vs* thin-skinned) across the mountain front, associated with the incorporation of the young and erodible proximal foreland basin sediments and shallowly-dipping thin-skinned structures, delivers a contrasting geomorphology between the main inboard orogenic body and its foothills within the piedmont zones.

The North Tehran Fault (NTF) in northern Iran is a major oblique-slip thrust fault which marks the southern mountain front of the central Alborz Range in the Tehran region. The enormous metropolitan area of the city, developed over the foothill-plain territory to the south of the NTF since 1554 (Ghassemi, 2023), includes geomorphological features which are produced by the interaction of active tectonic movements and proximal foreland deposition, and, therefore, provide crucial information for analyzing the seismic hazard of Tehran.

Our study is focused on and exploits field investigation, geomorphological examination and structural geological interpretation to provide information on the geometry, kinematics and morphological features of several active structures in the foothill territory of the Tehran region. We also used the recent microseismicity of the region to constrain the location and geometry of the active faulting in the Tehran piedmont zone. The studied Quaternary structures are the Kowsar, Mahmudieh, Davudieh, Chitgar and Ghurd-Daghi Faults and their corresponding hanging-wall folds and secondary faults. Our study combined luminescence dating to constrain the temporal interaction of the Quaternary faults and folds with the foreland sedimentation in the Chitgar Fault zone. The geochronological datasets were later employed to quantify the slip rate on some active faults generated in response to deformation over the main major active structure in the western Tehran area.

According to our findings, the foreland-involved structures in the Tehran region are dominantly inherited south-dipping faults – and related folds – which reached the surface in the Middle Pleistocene, and continued to act in the Late Pleistocene and Holocene. We discuss that these structures seem to still dynamically interact within the current kinematic framework of the southern Alborz region. The geometrical similarity and kinematic coherence of the piedmont zone faults reveal their association with a master active south-dipping fault at depth, here introduced as the ‘Master Ray Fault’. Materialization of such active fault, extending into the seismogenic depth in southern Tehran, can also explain the occurrence of several major enigmatic historical earthquakes in the Ray area, and, therefore, introduces a new potential seismic source for the Greater Tehran region.

2 Geological, tectonic and seismotectonic framework

The Alborz Range of northern Iran is an orocline which has evolved within the Arabia-Eurasia collision zone in the Cenozoic (Allen et al., 2003; Ballato et al., 2013; Mattei et al., 2017). Interaction of the rotating rigid South Caspian Basin basement with the orogen has deeply influenced the orogen, and appears to be causative of a transpressional tectonic setting across the orogen (e.g., Ballato et al., 2013; Ghassemi et al., 2023). The transpressional NTF system is the most prominent active structure at the southern mountain front in the Tehran region (Tchalenko, 1975) and is inferred to have kinematic links with the active Eastern Mosha Fault and the Buyin-Zahra Fault, respectively, to its east and west (Tchalenko, 1975; Ghassemi et al., 2016). The reverse dip-

https://doi.org/10.5194/egusphere-2025-500
Preprint. Discussion started: 1 July 2025

slip component of the movement on the NTF is estimated between 0.28±0.02 mm a^{-1} and 1.39±0.17 mm a^{-1} (Heydari and Ghassemi, 2025).

After a prelude compressional period associated with the Arabia-Iran collision in the Oligocene, the major uplift acts of the southern Alborz orogen were played in three Miocene time frames: 18-14 Ma, 9.5-7.5 Ma and 7-6 Ma (Ballato et al., 2013). The Miocene uplift events built colossal reliefs, which in turn constructed the southern foreland basin of the Alborz Range, and shed sediments of ca. 7 km thickness (the Upper Red Formation) into the basin (Ballato et al., 2008). The foreland sedimentation continued into the Pliocene and Quaternary and was associated with alluvial-fluvial deposition spanning as far as ca. 50 km south from the mountain front and beyond. The alluvial stratigraphy of the Tehran region established by Rieben (1955, 1966) is still in use by the urban geologists who work in the region, and includes the A, B, C and D Units. The oldest (?Pliocene to Middle Pleistocene) A Unit, also named informally Hezar-Darreh Formation, is the thickest (ca. 1200 m) and the most laterally continuous unit. For further detailed information on these alluvial-fluvial units' lithology and spatial distribution across the Tehran metropolitan area, see Ghassemi (2023).

Long-term geodetic monitoring since 2000 reveals 5±2 mm a^{-1} and 4±2 mm a^{-1}, respectively, for the shortening and shearing displacements across the Alborz Range (Vernant et al., 2004; Djamour et al., 2010; Khorrami et al., 2019). Most transpressional deformation is accommodated by the range-parallel thrust and left-lateral strike-slip structures, such as the NTF, Caspian Fault and Mosha Fault. However, the outward propagation of the deformation front has incorporated the foreland regions to the south and north of the orogen, and has produced prominent piedmont foothill landforms in the Pliocene and Quaternary sediments, which imply active deformation.

In spite of its association with major and minor active structures and accounts of several destructive historical earthquakes, the Greater Tehran region – including the NTF zone – lacks any instrumental period (1900-2024) seismicity greater than ca. 4.0 (e.g., Ashtari et al., 2005). This may reflect the locking of the active faults and/or the long return period of the major earthquakes on the crucial seismic sources in the region.

3 Morphology and structure of the Piedmont in Tehran

The piedmont zone in Tehran is a gently rolling small plateau extending between the mountain front along the NTF in the north and the northern margin of the Tehran plain in the south with the maximum and minimum elevations of respectively ca. 1850 to 1200 m a.s.l. (Fig. 1). Several generally east-west-trending hillocky landforms, developed over the folded and faulted A and B Units, dominate the piedmont zone and are incised by the major southward-flowing rivers.

Strong folding is dominant in the A Unit, while despite the faulting, the other three younger Units might only show some minor tilting. Stereographic analysis of the 97 bedding attitude measurements in the A Unit indicates almost pure north-south shortening direction and north-vergent folding associated with south-dipping thrust faults (Fig. 2). The north-dipping NTF and south-dipping faults described in this research appear to form a narrow intervening triangle zone structure in the north of the Tehran City.

https://doi.org/10.5194/egusphere-2025-500
Preprint. Discussion started: 1 July 2025

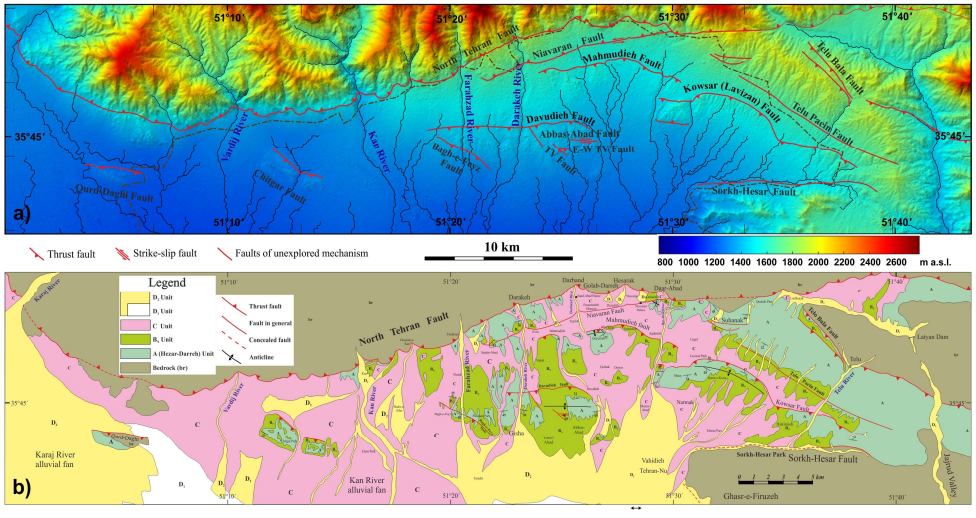

Figure 1: a) Distribution of the faults and the associated morphological features in the piedmont zone of the Tehran region. The faults are modified after Berberian et al. (1985). The background hillshade topographic map is SRTM DEM with a spatial resolution of 30 m. b) Geological map showing distribution of the alluvial units in the study area.

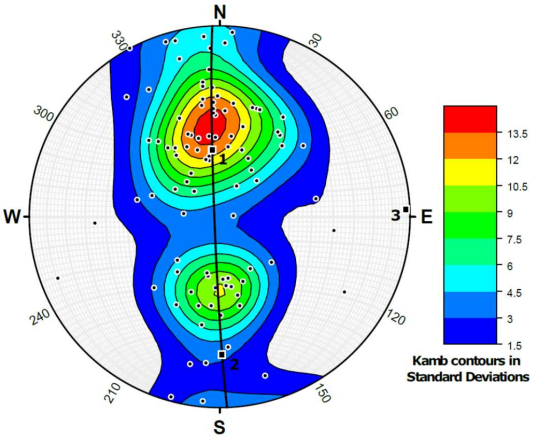

Figure 2: Kamb contour map of the poles to beddings in the A Unit (Hezar-Darreh Fm.) in the Tehran region. Point 3 on the stereogram illustrates the axis for the cylindrical best fit of the folding, showing an attitude of 02,089 (plunge, trend). As the diagram indicates, shortening after deposition of the A Unit has an almost sharp N-S orientation. The conspicuous asymmetry of the poles' distribution corresponds to the north-vergent folding and thrusting. The compasses used for the measurements were adjusted for 3° of magnetic declination in the Tehran region.

As observed on the structures depicted in Fig. 1, all five mapped major thrust faults in the piedmont, including the Kowsar, Mahmudieh, Davudieh, Chitgar and Ghurd-Daghi Faults, strike east-west to northwest-southeast and

https://doi.org/10.5194/egusphere-2025-500
Preprint. Discussion started: 1 July 2025

dip to the south. The sinuous surface trace of the faults suggests low-angle fault geometries. As we will discuss, these north-vergent thrusts in the piedmont region of the south-vergent NTF, instead of being kinematically related to the NTF, root in a major inherited bedrock structure within the Eocene volcanic rock sequence in the south of Tehran.

Some piedmont thrust faults are associated with the secondary minor faults in their hanging-wall. These include the north-dipping backthrusts, synthetic thrust faults parallel to the original fault, reverse faults oblique to the major thrust faults, and minor normal faults. Some examples are the backthrust on the western end of the Kowsar Fault, and the TV Fault and the East-West TV Fault in the hanging-wall of the Davudieh Fault (Fig. 1).

3.1 The Kowsar Fault

The Kowsar Fault (also named as the Lavizan Fault by some authors; e.g., Solaymani-Azad, 2023) is a shallowly-dipping west-northwest-striking thrust which places the A and B Units over the C Unit to the north (Fig. 3a). The surface trace of the fault extends as much as 15.5 km in the easternmost suburb of Tehran (Fig. 1). Applying the bow and arrow rule to the arcuate surface trace of the fault suggests a NNE direction of tectonic transport and 2.8 km of the horizontal component of displacement on the central part of this thrust fault (Fig. 1). Clear folding of the A Unit alluvial layers in the hanging-wall of this shallowly-dipping fault reveals a fault-bend folding mechanism for the deformation (Fig. 3b).

https://doi.org/10.5194/egusphere-2025-500
Preprint. Discussion started: 1 July 2025

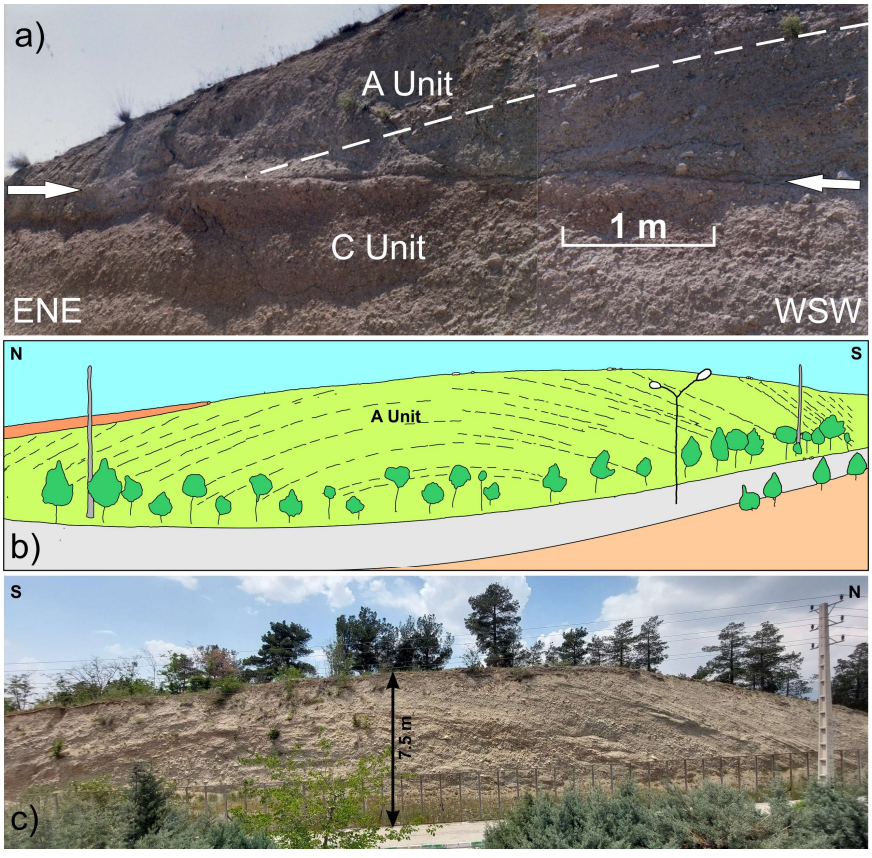

Figure 3: The Kowsar Fault in eastern Tehran. a) A roadcut trench along the Babaei Highway depicting the fault trace (arrows). Note the bedding in the A Unit, which represents a hanging-wall ramp on the C Unit. b) A hand-drawing illustrating the gentle folding of the A Unit layers in the hanging-wall of the Kowsar Fault in the Omid Town of the eastern Tehran. c) Photograph of the same fold as in (b), taken from the opposite side of the roadcut.

3.2 The Mahmudieh Fault

No outcrop of the Mahmudieh fault has been documented so far; however, according to the report by Berberian et al. (1985), this is a south-dipping fault which has formed a north-facing 10-15 m high scarp near its western termination. They suggest that the fault may be linked to the Kowsar Fault on its eastern termination. A major east-west structural depression has developed between the Niavaran Fault in the north and the Mahmudieh Fault in the south (Fig. 1).

3.3 The Davudieh Fault

The surface trace of the Davudieh Thrust Fault is 6 km long, and marks the northern margin of the folded and uplifted A Unit in the fault's hanging-wall. The TV Fault and East-West TV Fault, located in the hanging-wall of

https://doi.org/10.5194/egusphere-2025-500
Preprint. Discussion started: 1 July 2025

the fault, accommodate some shortening in addition to the deformation caused by folding and faulting on the master fault. The earlier secondary faults are named so due to their proximity to the Second National Iranian TV Station, which was the only nearby existing place in the area at the time of recognizing these faults (Berberian et al., 1985). The TV Fault is a high-angle reverse fault which strikes northwest-southeast and dips towards the southwest. In contrast, the E-W TV Fault dips towards the south (Fig. 4). The latter fault places the older impermeable A Unit over the younger B Unit. It forms a groundwater barrier, which was once manifested as a spring discharging of ca. 0.5 liters per second at a trench used for the construction of a ministry building. The Abbas-Abad Fault is another fault that has left-laterally displaced the morphological features developed by the Davudieh Thrust Fault. The surface trace of this east-west-striking fault is 2.2 km long, and its major slip component is strike-slip. Three South-discharging drainages, sculpted into the A Unit's alluvial deposits, are displaced by ca. 149, 197 and 286 m, averaging 211 m (Fig. 4b).

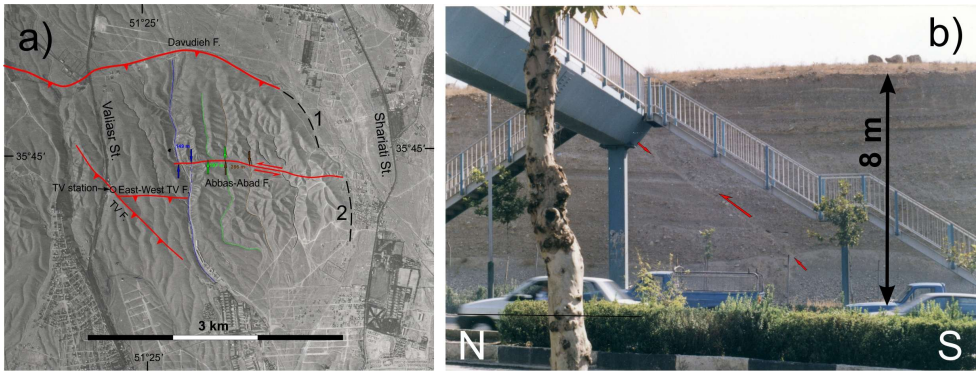

Figure 4: a) The Davudieh Thrust Fault and the associated secondary faults in its hanging-wall. The colored arrows illustrate drainage restoration along the Abbas-Abad Fault and indicate an average of 211 m left-lateral strike-slip displacement. Note the similar displacement of the uplifted landform produced by thrust movement on the Davudieh Fault (black dashed lines 1 and 2). The aerial photographs used in this figure, figures 5 and 7, belong to 1955. b) Outcrop of the East-West TV Fault on a roadcut in the Mandela Blvd. The fault displaces the B Unit on the surface and places the A Unit over the B Unit a few meters below the street's level.

The Davudieh Fault, first introduced by Berberian et al. (1985), is a major south-dipping thrust, the surface trace extending for ca. 12 km in the north-central Tehran region. In addition to the structures above, the fault is associated with a strong open to tight asymmetric folding in the alluvial A Unit, as well as local normal faulting (Fig. 5). Thickening of the hanging-wall layers towards the aforementioned normal faults suggests syn-sedimentary faulting during deposition of the B Unit (Fig. 5b).

Fault-related folding of the A Unit in the hanging-wall of the Davudieh Fault is essentially similar to what is already described for the Kowsar Thrust Fault. The resultant uplift of the relatively erosion-resistant alluvial materials in the A Unit has produced east-west-trending hillocky morphology that is generally occupied by parks and vegetated greenways (e.g. Pardisan Park). The active folding in the hanging-wall of the Davudieh Fault has

https://doi.org/10.5194/egusphere-2025-500
Preprint. Discussion started: 1 July 2025

resulted in a maximum of ca. 70 m of incision of the Farahzad River into the B Unit (Ghassemi, 2023). The morpho-structural feature in the Pardisan area was interpreted as folding in a foreberg by Ritz et al. (2012) and as the recently introduced north-dipping Pardisan thrust Fault by Talebian et al. (2016). We will discuss such kinematic interpretations in Section 5.

Another interesting manifestation of the active deformation in the hanging-wall of the Davudieh Fault is the Bagh-e-Feyz Oblique-Slip Fault (Figs. 1 and 5a). The fault strikes NW-SE and dips 40° towards the southwest (Fig. 6). The curved 3.4 km long surface trace of the fault is probably related to a local block rotation. The minimum dip-slip component of movement on the fault exposed in an outcrop is ca. 12 m (Fig. 6), while three drainage talwegs on the aerial photographs are right-laterally displaced by the fault as long as ca. 92, 41 and 83 m (Fig. 5a). A small relatively fresh drainage divide, probably related to a more recent period of activity, represents ca. 27 m of right-lateral displacement across the fault (inset in Fig. 5a).

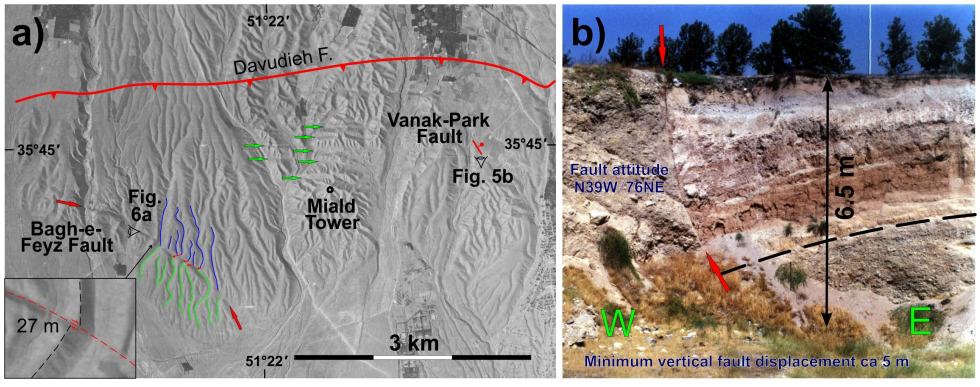

Figure 5: a) Structural features in the hanging-wall of the Davudieh Fault. A normal fault of the Vanak-Park Fault system is illustrated in 5b. The green arrows delineate the grooves sculpted in the landscape due to the tightly folded and steep A Unit's alluvial layers. Drainages across the Bagh-e-Feyz Fault show a minor component of right-lateral movement on the fault. The inset is an enlarged image of a ridge displaced by ca. 27 m. b) Outcrop of a listric normal fault from the Vanak-Park Fault system displacing the shallowly-dipping B Unit. Note the thickening of some hanging-wall layers approaching the fault.

https://doi.org/10.5194/egusphere-2025-500
Preprint. Discussion started: 1 July 2025

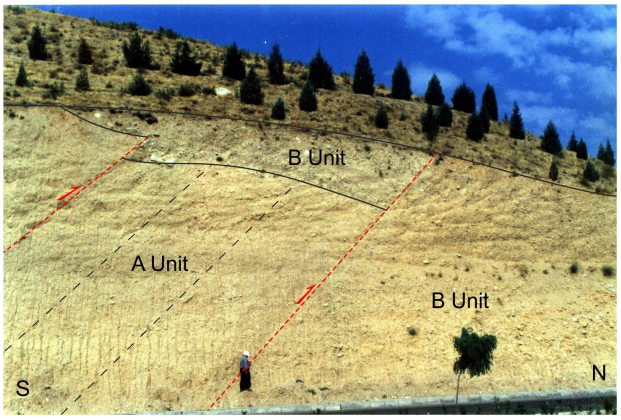

Figure 6: Outcrop of the Bagh-e-Feyz Fault on a highway roadcut in western Tehran. The A Unit's layering in the hanging-wall is parallel to the fault. Note a secondary reverse fault in the hanging-wall. The person in the image is for scale is 170 cm tall.

3.4 The Chitgar Fault zone

Near the western end of the Tehran metropolis, the Chitgar Hills display another significant structural complex linked to the south-dipping thrust faulting in the piedmont zone of the city. The highway roadcuts excavated in 2008 revealed a major thrust fault that roots in the Eocene volcanic bedrock and places it – and the overlying A Unit – over the A Unit – and the overlying horizontal layers of the B Unit alluviums (Figs. 7a, 8d). The resultant fault-bend folding in the alluvial materials has produced a major bipartite hill, which, akin to the hills in the hanging-walls of the Kowsar and Davudieh Faults, hosts parks and vegetated greenways. The western and eastern parts of the hill trend NW-SE and WNW-ESE respectively possibly due to a spatial change in the underlying fault ramp geometry at the intersection of an oblique ramp and a frontal ramp of the Chitgar Thrust (Fig. 7b). Separation of the two parts and the intervening inferred normal faults may have evolved due to out-of-plane displacement near the trailing termination of the oblique ramp resulted in local lateral extension of the hanging-wall (e.g., Apotria, 1995).

The Chitgar Thrust demonstrates a prominent and relatively fresh fault scarp on the northern rim of the eastern Chitgar Hills (Fig 7b). From the south to the north, the following features are observed along a highway roadcut across the Chitgar Fault-related folding structure (Fig. 8): 1) The growth strata of the more recent B or C Unit over an unconformity above the folded and faulted A Unit. 2) A backthrust zone in the hanging-wall of the Chitgar Thrust showing few meters of displacements. 3) The main south-dipping Chitgar Fault, which thrusts the bedrock Eocene volcanic rocks over the A Unit. 4) A zone of reverse and inverted normal faults within the B Unit. 5) A zone of oblique-slip normal faults within the B Unit. Construction of a semi-balanced cross section for the western part of the Chitgar structure (Fig. 8d) prescribes ca. 1047 m and 68 m of pre- and post-B Unit displacement on the fundamental thrust.

The B Unit covers a relatively small low-relief northwestern terminal portion of the fault-bend folded layers of the A Unit (Fig. 7b). We suggest that such a morpho-depositional setting has been resulted from beveling of the

https://doi.org/10.5194/egusphere-2025-500
Preprint. Discussion started: 1 July 2025

fault-bend fold and deposition of the B Unit by an old river; for a detailed example of the processes responsible for such lateral erosion and deposition (gravel-covered planation surface) over growing folds (see Bufe et al., 2017).

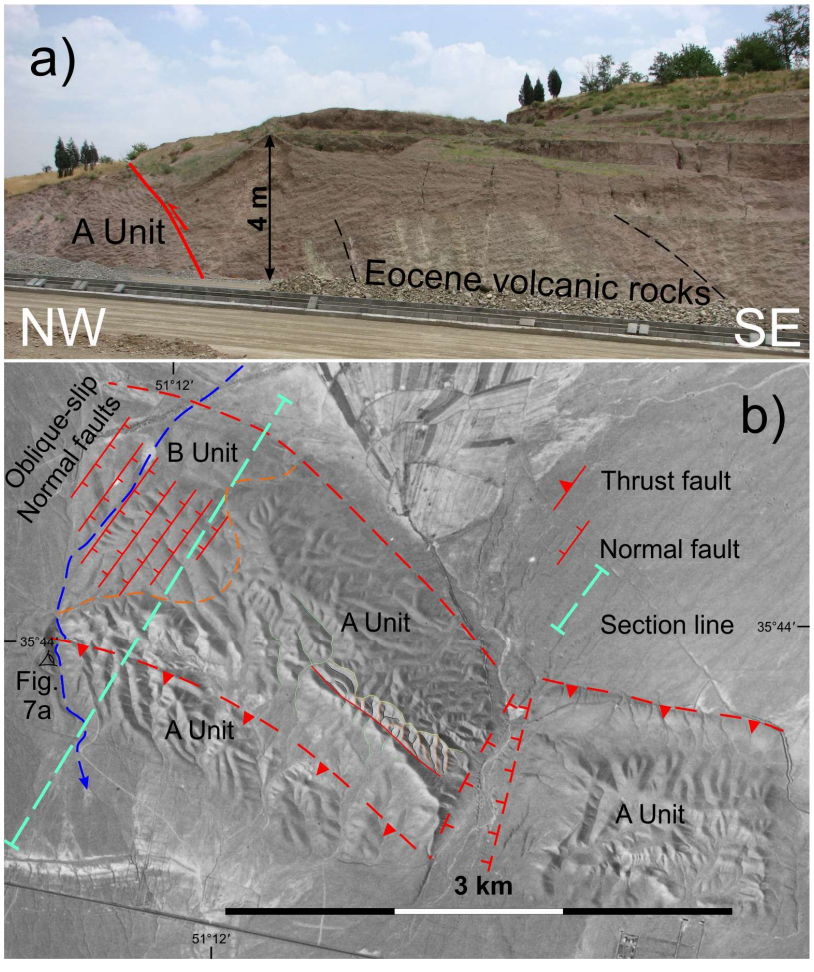

Figure 7: a) The Chitgar Thrust Fault ramp on a roadcut west of the Chitgar Park. The Eocene volcanic layers parallel to the ramp reveal a hanging-wall flat. The volcanic rocks were not exposed before the roadcut trenching. b) The bipartite hill morphology developed over the Chitgar Thrust Fault, manifesting a complex ramp structure. The oblique-slip normal faults on the western end of the hills within the B Unit are drawn schematically. The blue dashed line represents an old river course presumably responsible for the beveling of the fault-bend fold and deposition of the B Unit in this area. Note the sharp fault scarp of the Chitgar Thrust on the northern margin of the eastern Chitgar Hills.

https://doi.org/10.5194/egusphere-2025-500
Preprint. Discussion started: 1 July 2025

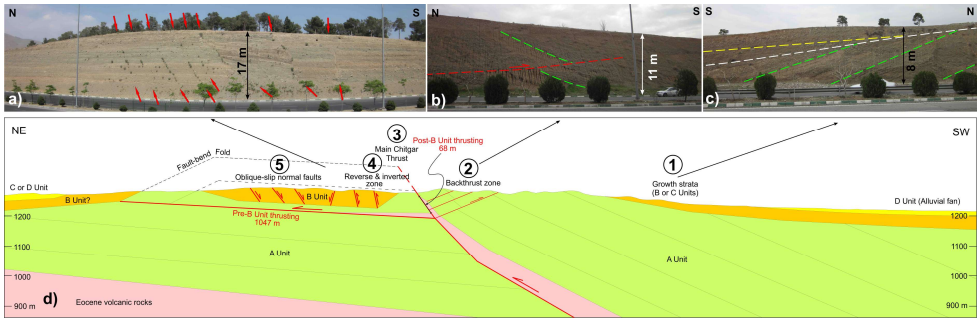

Figure 8: Structural setting of the Chitgar area of western Tehran. a) Oblique-slip normal faults within the extended and inverted zone of the B Unit. The fault traces are generally delineated by the linear growth of the thornbushes (red arrows). b) A backthrust in the hanging-wall of the main Chitgar Thrust displacing alluvial layers of the A Unit. c) Growth strata of the B or C Unit over the folded layers of the A Unit. d) Semi-balanced cross section of the Chitgar area. The section line is shown in Fig. 7b.

The backthrust zone encompasses shallowly-north-dipping minor thrust faults of a few meters displacement in the A Unit (Fig. 8a). These faults appear to accommodate the localized thrust sheet deformation during its passage over the ramp; a phenomenon observed in analogue modelling of thrust systems (e.g., Rosas, 2017).

The southern exposures of the B Unit in the Chitgar area show a zone of minor reverse faults in the footwall vicinity of the Chitgar Thrust. About eight faults in this zone dip steeply to the NNE, are ca. 1.5 to 4 m apart, and display reverse displacements of ca. 2-12 cm. Two measured faults of this set strike NW-SE, parallel to the strike of the Chitgar Thrust, testifying to a dynamic relationship between the major thrust fault and the minor faults (Fig. 9a). This compressional fault zone gives way to an extensional zone of faulting towards the north. However, a half-graben developed in the latter zone appears to be inverted by the more recent compressional event (Fig. 9b).

Towards the north, the extensional oblique-slip faulting dominates within the sub-horizontal layers of the B Unit. The slight angle of the faults relative to the N-S roadcut wall, inhomogeneity of the alluvial layers in the B Unit, and the strike-slip component of the movement on the faults have resulted in irregular exposures of the fault trace along the studied section (Fig. 10). The curvilinear pattern of the faults may be partially related to the large-scale ridge and groove structure commonly reported on much smaller scales from the fault planes elsewhere (e.g., Lin and Williams,1992).

Orthographic analysis of the 155 cm long apparent dip-slip movement observed on the trench wall oblique to a measured oblique-slip fault plane reveals 131.5, 258.1 and 289.7 cm of, respectively, normal dip-slip, left-lateral strike-slip and net-slip movements on the fault (Fig. 10c).

3.5 The Qurd-Daghi Fault

The westernmost fault in the Tehran piedmont region is the Qurd-Daghi Fault. Similar to all other thrust faults in the piedmont region, the fault dips towards the south and places the Eocene volcanic bedrock onto the A Unit in

https://doi.org/10.5194/egusphere-2025-500
Preprint. Discussion started: 1 July 2025

its footwall. The surface trace of this east-west striking fault is 4.2 km long, and occurrence of the south-dipping A Unit above the Eocene bedrock in the hanging-wall confirms the dip direction of the fault.

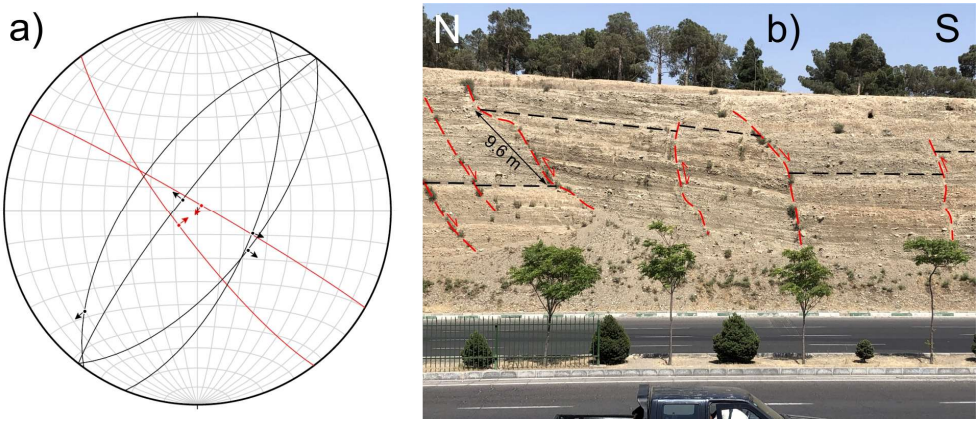

Figure 9: a) Stereographic projection of the faults measured in the B Unit of the Chitgar area. The red great circles are reverse faults which are parallel to the major Chitgar Thrust. B) A half-graben in the B Unit inverted by the later compressional event induced by thrusting. Note that in case of simple half-graben development, the layers' rotation should demonstrate an opposite sense. The apparent dip-slip movement on the inverted fault is 9.6 m.

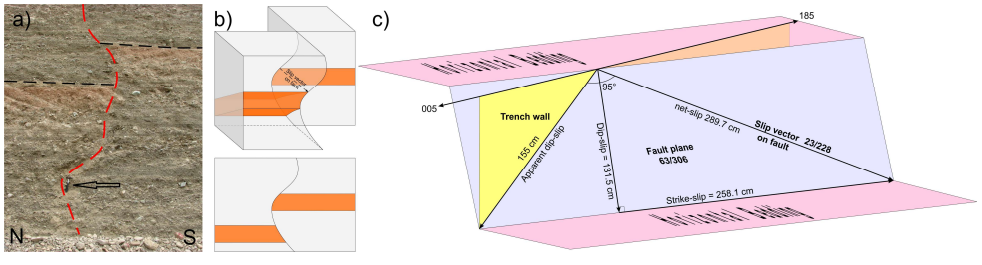

Figure 10: Geometry and kinematics of the faulting in the extended zone of the Chitgar area. a) The curvilinear geometry of the oblique-slip normal faulting in the alluvial B Unit. Hammer for scale (arrow) is 31 cm long. b) Conceptual model of the movement along a slip vector, which is parallel to the fault's ridge and groove axes and oblique to both the layering and the trench wall surface. The lower panel illustrates the resulting section after trenching. c) Orthographic reconstruction of an oblique-slip left-lateral normal fault in the Chitgar section. The apparent dip-slip movement measured on the trench wall is sequentially resolved into dip-slip and strike-slip components of movement and then into a net-slip vector on the fault plane.

4 Luminescence dating of alluvial materials in the Chitgar area

Due to a good exposure of the faulting and folding in the Quaternary alluvial deposits of the Chitgar area in a roadcut trench of western Tehran, we planned sampling of the outcropped sediments to evaluate the intricate

https://doi.org/10.5194/egusphere-2025-500
Preprint. Discussion started: 1 July 2025

faulting and sedimentation history in this crucial area of piedmont deformation. The outcropped alluvial sequence of the B Unit here consists of horizontal layers of gray poorly sorted gravels in a sand size matrix, which includes a few brick-red to pale brown paleosol horizons. We took four sediment samples from B Unit to apply optically stimulated luminescence (OSL) dating (Huntley et al.,1985). The locations of these sediment samples are shown in Fig. 11. The sediments were prepared using common procedure for luminescence dating (Preusser et al., 2008). We extracted polymineral fine-grain fraction (4-11µm) to date the samples using post-infrared stimulated luminescence (pIRIRSL) at 225 °C ($pIRIRSL_{225}$) after the protocol setting of Buylaert et al. (2009). This grain size was selected as the coarser ones (100-150 µm) led to dim signals hampering accurate measurements. The measurement protocol was modified to obtain satisfactory dose recovery ratios for samples Ch2 and Ch4. The single saturating exponential plus linear function fits the datasets and generates the dose-response curve. The late background subtraction was employed to extract the signal of interest. The arithmetic average and the standard error of the mean were calculated to represent the equivalent dose (D_e) and its error (Table 1). The data analysis was performed using the R (R Core Team, 2023) "luminescence" package (Kreutzer et al., 2023, 2012).

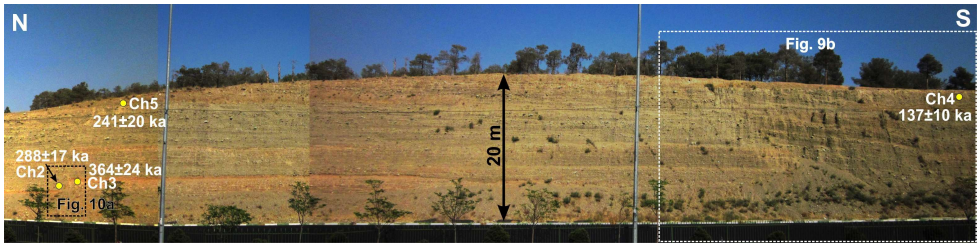

Figure 11: Locations of the samples Ch2-5 on the Chitgar roadcut. Maximum thickness of the outcropped sediments in the middle of the photograph is ca. 22 m.

The environmental dose rates were estimated using radionuclide concentrations obtained from low-background gamma-ray spectrometry at VKTA in Dresden, Germany. These values were corrected for the grain size and converted to the dose rates after Guérin et al., 2011; Guérin and Mercier, 2012. The a-value of 0.11 ± 0.02 was employed for the polymineral fraction following Kreutzer et al. (2014). The estimated dose rates were then corrected for water attenuation. The saturated water content was determined using granulometry results (Nelson and Rittenour, 2015). The fraction of 0.50±0.20 of the saturated water content was used to approximate the past water content of the sediment. The geographical coordinates and the overburden depth were used to calculate the cosmic dose rate estimates (Prescott and Hutton, 1994; Prescott and Stephan, 1982). Internal dose rates were calculated with the presumption of 12.5 ± 0.5 % K concentration in polymineral fine-grain samples (Huntley and Baril, 1997). The final dose rates were calculated using the online calculator DRAC v1.2 (Durcan et al., 2015).
We have measured the laboratory fading for $pIRIRSL_{225}$ for two samples Ch2 and Ch4, which exhibited 0.93 ± 3.9 % per decade ($g\text{-value}_{2days}$) and 1.01 ± 2.54 per decade ($g\text{-value}_{2days}$), respectively. Therefore, the obtained ages were not corrected for the laboratory fading. This observation was in line with the previous luminescence dating study on the NTF in northern Tehran which showed no considerable fading for the same signal (Heydari et al., 2024).

https://doi.org/10.5194/egusphere-2025-500
Preprint. Discussion started: 1 July 2025

It should be noted that the ages, mainly Ch2, Ch3 and Ch5, can be considered underestimated as the D_es lie between 1052 to 1386 Gy, which seems to be above the upper limit for the pIRIRSL signal (Heydari et al., 2022, Zhang and Li, 2020). This range is at the non-linear part of the dose-response curve close to the saturation, and as such, the obtained D_e tends to underestimation, and its error might not be trustworthy (Duller, 2007; Heydari and Guérin, 2018).

Nevertheless, given the nature of the alluvial deposits, the possibility of insufficient bleaching cannot be excluded (Heydari et al., 2020). Therefore, our ages might be interpreted as maximum ages. However, it is worth considering that the ages systematically follow the stratigraphy, and get older as the depth increases. This could indicate that it is likely that the alluvial materials were bleached before deposition, yet it is unclear to what extent bleaching happened.

Table 1: The Chitgar area luminescence ages using polymineral fine-grain fraction (4-11 µm). The $pIRIRSL_{225}$ signal was used for signal measurements.

Sample	D_e (Gy)	σ	D_r (Gy/ka)	σ	Age (ka)	σ
Ch2	1284	25	4.46	0.22	288	17
Ch3	1386	29	3.81	0.23	364	24
Ch4	615	25	4.50	0.25	137	10
Ch5	1052	50	4.37	0.28	241	20

- D_r is the environmental dose rate, and D_e is the equivalent dose.

Samples Ch3 and Ch5 were taken respectively near the bottom and top of the outcropped B Unit and were used to estimate a time-averaged alluvium sedimentation rate of the unit, which was 0.1 mm a^{-1} (more precisely reported as 0.095 mm a^{-1}). Sample Ch4, was taken from the topmost alluvial sequence to constrain the end of the B Unit deposition, which yielded an OSL age of 137±10 ka. Since the extensional oblique-slip faults cut the whole sequence, dividing the net-slip movement on the well-constrained fault, described in Fig. 10, by the abovementioned age reveals a minimum slip rate of 0.02 mm a^{-1} for this fault.

The major inverted oblique-slip normal fault in the B Unit shows 9.6 m of apparent reverse slip in the Chitgar roadcut (Fig. 9b). The fault appears to be incipiently responsible for the development of a half-graben during the extensional event that affected the B Unit. However, the later compressional deformation in the footwall of the Chitgar thrust has caused its inversion and reverse movement. Dividing the aforementioned apparent reverse slip by the minimum age of the faulted B Unit (137±10 ka) and ignoring the early normal component of movement results in a minimum slip rate of 0.07 mm a^{-1} for the fault.

The total thickness and age range of the B Unit in the Chitgar area are of major importance for estimating the slip rate on the Chitgar Thrust Fault. Considering the geometric and kinematic model of the fault (Fig. 8d), we may consider a pre-B Unit slip (1047 m) whereby the original fault-bend fold developed and a post-B Unit slip (68 m),

https://doi.org/10.5194/egusphere-2025-500
Preprint. Discussion started: 1 July 2025

which has cut the backlimb of the fold. Considering the maximum age for deposition of the B Unit (137±10 ka), the minimum slip rate for the second period of slip on the Chitgar Thrust would be 0.50 mm a^{-1}.

5 Microseismicity in the Tehran region

As explained under Section 2, the limited instrumental period seismicity in the Tehran region is inconsistent with the occurrence of the major and minor active faults inside and around the metropolitan area. We analyzed the region's earthquake catalogue, which was provided by the Iranian Seismological Center (IRSC), Geophysics Institute, and the University of Tehran. The catalogue includes the recent seismicity spanning between January 2006 and December 2024 (19 years), and reveals the following characteristics of the microearthquakes (Fig. 12):

a) The earthquakes are small in size (magnitudes between 1.0 and 4.0 – Nuttli magnitude scale), but frequent in occurrence (449 events in 19 years).

b) The reported event depths range from the near-surface to a maximum depth of ca. 20 km.

c) The number of the events located in the north of the NTF's surface trace are markedly less than those located in its south.

d) The microearthquakes show a dense population in the eastern part of Tehran as compared to elsewhere in the region.

e) Fitting a 2D polynomial surface of degree 2 using the linear least squares to the reported earthquake hypocenters divulges a potential gently-south-dipping source at a depth of ca. 10 km.

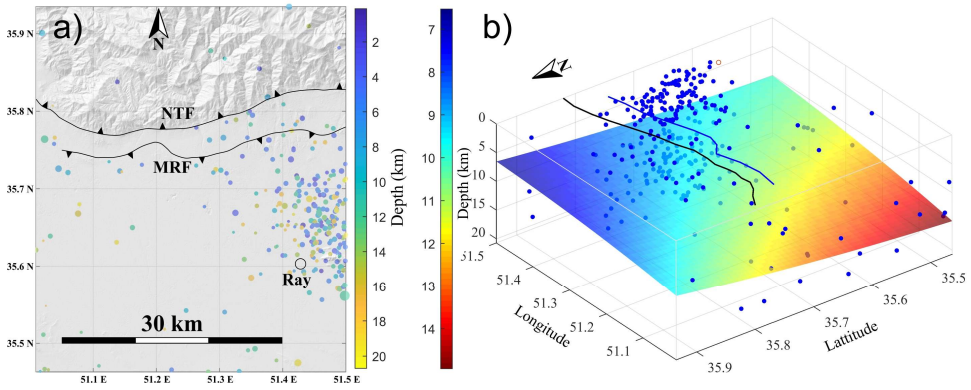

Figure 12: Recent (2006-2024) microseismicity in the Tehran region. a) Map view. Note the scarcity of the events in the hanging-wall of the Nort Tehran Fault (NTF) and clustering of the events in the eastern part of the city (hanging-wall of the Master Ray Faut – MRF). The events' focal depth and magnitude (1.0 to 4.0) are shown by the points' color and size, respectively. b) Three-dimensional view. The best fit to the earthquakes' hypocenters is shown as a gently-south-dipping surface spanning at depths of ca. 7 to 15 km. The black and blue lines at the surface indicate the locations of the NTF and MRF, respectively. The Ray city in the south of Tehran is shown as a red circle both on (a) and (b).

https://doi.org/10.5194/egusphere-2025-500
Preprint. Discussion started: 1 July 2025

6 Discussion

The piedmont region of the Tehran metropolitan area is dominated by five major south-dipping thrust faults, namely the Kowsar, Mahmudieh, Davudieh, Chitgar and Qurd-Daghi Faults, and their related hanging-wall structures, which generally expose the Pliocene-Pleistocene A and B Units and the subjacent Eocene volcanic bedrock as elongated hillocky landforms. The south-dipping north-vergent faulting contrasts with the generally south-vergent and transpressional structural grain of the southern Alborz Range (e.g., Allen et al., 2003; Ballato et al., 2013). However, some studies document major south-dipping faults in the southern Alborz region. For example, Ballato et al. (2008) introduce a south-dipping fault in the core of a north-verging fault propagation fold (the Southern Alborz Anticline) located in the Eyvanekey area to the southeast of Tehran. Our findings defy and refute the north-dipping foreberg model (Ritz et al., 2012) and the Pardisan Thrust Fault model (Talebian et al., 2016), which tries to explain the causative active structure for the development of the ridge in the hanging-wall of the south-dipping Davudieh Fault. The sediment sample taken for OSL dating and slip-rate estimate of the Pardisan Fault in Talebian et al. (2016), in fact, resides on the hanging-wall of the Bagh-Feyz south-dipping oblique-slip fault. Therefore, the age of this sample might be used to estimate the slip rate on the latter fault.

Statistical analysis of the bedding attitudes in the A Unit of the Tehran region reveals asymmetric north-vergent folding associated with south-dipping thrust faults. The north-facing cumulative escarpments on the piedmont faults and the gentle dip-slopes on gently-dipping backlimb structures comply with the dominance of the north-vergent thrusting in the piedmont region. According to our observations, the north-dipping south-vergent thrusting in the piedmont is much smaller and is limited to the close vicinity (ca. 1 km) of the North Tehran Fault at the mountain front. As a result, a triangle zone may be envisaged between these oppositely verging thrust faults in the northern rim of the piedmont zone.

The south-dipping north-vergent thrust faults may be provisionally considered as the structures inherited from the early stages of the Alborz orogeny in the Oligocene or Early Miocene times before the development of south-vergent retrowedge in the hinterland of the orogen.

The en échelon and partially overlapping array of the Kowsar, Mahmudieh and Davudieh Faults (Fig. 1) imply the transfer zones where these thrust faults die out, and their displacement is transferred onto the neighboring faults (e.g., Dahlstrom, 1970).

Recognition of the active south-dipping thrust faults in the piedmont region of Tehran and understanding their geometry and kinematics are of major relevance to the comprehensive seismic hazard investigation of the Tehran metropolitan area. We present evidence for the involvement of the bedrock in the faulting, and as such, we suggest that the faults extend into the seismogenic layer in southern Tehran.

6.1 The newly defined “Master Ray Fault”

The ancient city of Ray (Rhagae) was the predecessor of the recently flourished Tehran city (since ca. AD 1554) and was entirely engulfed by Tehran after the 1970s (e.g., Ghassemi, 2023). Historical accounts affirm the devastation of Ray by some major earthquakes, and the city even received the name (Rhagae) because its land surface had been rent by earthquakes in the eastern part, and numerous towns and villages were destroyed (Strabo, 1969). The ruined city was reportedly rebuilt by Seleucus Nicator (Starbo, 1969) in 312-280 BC. Ambraseys and

https://doi.org/10.5194/egusphere-2025-500
Preprint. Discussion started: 1 July 2025

Melville (1982) suggested that this major historical event (Mw≥7.0) must have occurred after Alexander's passage through Rhagae in 330 BC, during the reign of Seleucus. The authors also believed that the reported devastation may refer to more than one earthquake. Two further historical records of destructive earthquakes, with estimated moment magnitudes of 7.0 and >6.0 in AD 855 and AD 864, respectively (Berberian and Yeats, 2016), reveal a very high potential for the seismic hazards in the Ray area of southern Tehran. A light earthquake (Mw = 4.3) occurred on October 17, 2009, east of Ray at a centroid depth of ca. 12 km and has shown almost a pure reverse mechanism (Yaminifard et al., 2012). Such recent seismotectonic data are rare; however, they may provide useful insight into the geometry, kinematics, and possible depth range of potential earthquakes in the Ray region of Tehran. Occurrence of the historical and instrumental period earthquakes in the Ray region has been differently ascribed to the North Ray, South Ray, Kahrizak and Parchin Faults (e.g., Berberian and Yeats, 2016). Most of these faults show surface traces very close to Ray City, and hence, considering a finite dip for these faults, which are generally of reverse mechanism, demands macroseismic epicenters a couple of 10 km distant from the city in the north or south. Although it is worth noting that such distances between the epicenters of the past major earthquakes and the ancient city of Ray could not certainly prevent the destruction of the city, as the ancient constructions were not likely designed to be earthquake-resistant. Nevertheless, as an alternative solution, we propose that the south-dipping thrust faults in the piedmont region of Tehran (i.e., Kowsar, Davudieh, Mahmudieh, Chitgar and Qurd-Daghi) manifest a major active fault on the surface that provides the earthquake source at the seismogenic depth for the Ray region (Fig. 13). We name this active fault the 'Master Ray Fault' and suggest that it has to be considered a major earthquake source to evaluate the seismic hazards in the Greater Tehran region. The Master Ray Fault described here differs from the North Ray and South Ray Faults introduced by Berberian et al. (1985). As a parallel interpretation, the occurrence of major earthquakes on such fault can cause surface rupture hazards on the studied Quaternary faults dispersed in the piedmont zone of the highly populated northern Tehran area, where important vulnerable lifelines and residential areas would be affected. Both the Master Ray Fault and its surface counterparts in northern Tehran may be potentially active in the current roughly north-south shortening kinematic framework of northern Iran.

Study of the microseismicity of the Tehran region uncloak a gently-south-dipping seismic source at an average depth of ca. 10 km. This hypothetical surface is geometrically coherent with our model of the seismogenic Master Ray Fault. The frequent microseismicity, specially on the eastern portion of the Master Ray Fault, notifies the moment release on the fault which may be associated with some corresponding (aseismic) creep (e.g., Gans and Furlong, 2003).

According to our interpretation based on the thrust fault geometries in the piedmont zone, the Master Ray Fault has a minimum surface trace length of 57 km. We suggest that due to the shallowly dipping expression of the fault, its maximum dip at the seismogenic depth would be ca. 30°.

Considering the calculated slip rate on the Chitgar Thrust to be representative of the slip rate on the Master Ray Fault, and using the average displacement-magnitude relationship of Wells and Coppersmith (1994), the average return period for the earthquakes of moment magnitude 7.0 for this important seismic source would be ca. 1,321 years.

https://doi.org/10.5194/egusphere-2025-500
Preprint. Discussion started: 1 July 2025

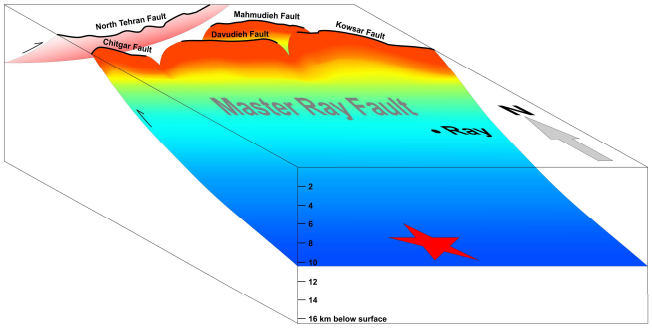

Figure 13: A conceptual model for the geometry of the Master Ray fault, and its connection to the piedmont zone faults at depth. Reaching the seismogenic depth in the south, the fault is capable of producing major earthquakes for the Ray City and the southern Tehran metropolitan area. The red star represents a hypothetical hypocenter on the fault plane.

7 Conclusion

The uplifted and incised piedmont region of northern Tehran furnishes a unique opportunity to study active structures and the related seismic hazard within the metropolitan area of this exceptionally vast and highly populated capital city. Such an abundance of exposed surface faulting in the city overrules the general scarcity of surface ruptures associated with the thrust faults (e.g., Ghassemi, 2016). Five south-dipping thrust faults of variable surface trace lengths have created eminent fault-related folding and the related secondary structures in the region, which accommodate the north-south shortening in the southern foothills of the central Alborz Range. In addition to the folding, other active structures in the hanging-wall of the major thrust faults, including the reverse, normal, strike-slip and backthrust faults, as well as growth strata, reveal a complex deformation history for the piedmont zone in the Quaternary.

The asymmetric north-vergent folding in the alluvial A Unit, the field evidence for the south-dipping thrust faults, and the microseismicity data point to a major south-dipping fault, which is manifested as several subsidiary surficial active structures in the piedmont zone of Tehran region. Our model for the kinematics of the aforementioned piedmont structures contends some recent interpretations of the piedmont structures being developed by the south-vergent north-dipping thrust faults associated with the movement on the NTF (e.g., Talebian et al., 2016), as such interpretations can have an essential bearing on the trustworthy assessment of the seismic hazard for the densely populated Tehran metropolitan area.

The Chitgar Thrust Fault in western Tehran is associated with a combination of fault-bend folding, growth strata, backthrusts, minor reverse faults, oblique-slip normal faults and beveling of the folded A Unit, which make this area a pragmatic lab for the study of the Quaternary deformation in the piedmont zones.

The OSL dating of the B Unit alluvial materials in the Chitgar area implies an average 0.1 mm a^{-1} rate of deposition for the B Unit and minimum and maximum ages of respectively 137±10 and 364±24 ka for the exposed section of the B Unit in this part of Tehran.

https://doi.org/10.5194/egusphere-2025-500
Preprint. Discussion started: 1 July 2025

Our kinematic analyses, along with the luminescence-based chronology, provide a small slip rate on the order of 0.02 and 0.07 mm a^{-1}, respectively, for an oblique-slip normal fault and an inverted normal fault of the Chitgar Hills area. Moreover, the minimum slip rate of the Chitgar Thrust after deposition of the B Unit is calculated to ca. 0.50 mm a^{-1}. Therefore, we expect the cumulative slip rate of the secondary faults in the Chitgar area – and elsewhere in the piedmont zone – to be less than 0.5 mm a^{-1} estimated for the Master Ray Fault.

Geometrical and kinematic analyses of the actively deforming south-dipping thrust faults in the piedmont region of Tehran, in combination with the data on historical seismicity of the southern Tehran region as well as the microseismicity information of the region, have led us to introduce the 'Master Ray Fault' as an important seismic source for the Ray City, and therefore for the Greater Tehran region. Seismic activity on such a crucial thrust fault may lead into surface rupture hazard of the piedmont zone faults which cross the foundations of the city in its northern half. The dominance of south-dipping thrust faults, and the asymmetry of folding in the alluvial A Unit comply with north-vergent tectonic transport direction, and defies the recent interpretation of the south-vergent active faulting in the piedmont region of Tehran.

Our study establishes a critical methodological framework to advance the understanding of Quaternary thrust fault kinematics and their geomorphic signatures, while also addressing and rectifying misinterpretations in existing analyses of these structures. This framework enhances the identification and assessment of potential seismic sources in densely populated metropolitan regions situated within piedmont zones near active orogenic belts, contributing to improved seismic hazard evaluation.

Acknowledgements

MH received funding from the Alexander von Humboldt Foundation (#FRA 1221685 HFST-P). This study was further supported through the DFG grant #507272784. MRG is thankful to the Research Institute for Earth Sciences, Geological Survey of Iran, for the granting of the opportunity for this research work and the fieldwork assistance. We are also grateful to Dr. N. Mirzaei of the Iranian Seismological Center (IRSC), Geophysics Institute, University of Tehran, for providing us with the microseismicity data of the network in Tehran.

Data Availability Statement

The SRTM 30 m topographic data used to produce the hillshade in Fig. 1 are available at https://www.earthdata.nasa.gov. The hillshade and related drainage network in Fig. 1 is created using the TopoToolbox 2 – MATLAB-based software (Schwanghart and Scherler, 2014). The Kamb contour map in Fig. 2 is created using Stereonet 11 (Allmendinger et al., 2013), available at https://www.rickallmendinger.net/stereonet.

References

Allen, M.B., Ghassemi, M.R., Shahrabi, M., and Qorashi, M., 2003. Accommodation of late Cenozoic oblique shortening in the Alborz range, northern Iran. Journal of Structural Geology, 25(5), 659–672.

https://doi.org/10.5194/egusphere-2025-500
Preprint. Discussion started: 1 July 2025

520 Allmendinger, R.W., Cardozo, N.C., and Fisher, D., 2013. Structural geology algorithms: Vectors and tensors.
521 Cambridge, England, Cambridge University Press, 289 p.

522 Ambraseys, N.N., and Melville, C.P., 1982. A history of Persian earthquakes, Cambridge University Press,
523 Cambridge. 240 p.

524 Apotria, T.G., 1995. Thrust sheet rotation and out-of-plane strains associated with oblique ramps: An example
525 from the Wyoming salient, U.S.A. Journal of Structural Geology, 17(5), 647-662.

526 Ashtari, M., Hatzfeld, D., and Kamalian, N., 2005. Microseismicity in the region of Tehran. Tectonophysics, 395
527 (2005), 193-208.

528 Ballato, P., Nowaczyk, N.R., Landgraf, A., Strecker, M.R., Friedrich, A., and Tabatabaei, S.H., 2008. Tectonic
529 control on sedimentary facies pattern and sediment accumulation rates in the Miocene foreland basin of
530 the southern Alborz mountains, northern Iran. Tectonics, 27, TC6001, doi:10.1029/2008TC002278

531 Ballato, P., Stockli, D.F., Ghassemi, M.R., Landgraf, A., Strecker, M.R., Hassanzadeh, J., Friedrich, A., and
532 Tabatabaei, S.H., 2013, Accommodation of transpressional strain in the Arabia-Eurasia collision zone: new
533 constraints from (U-Th)/He thermochronology in the Alborz mountains, north Iran. Tectonics, 32, 1-18,
534 doi: 10.1029/2012TC003159.

535 Berberian, M., and Yeats, R.S., 2016. Tehran: An earthquake time bomb. In: Sorkhabi, R., (ed.), Tectonic
536 Evolution, Collision, and Seismicity of Southwest Asia: In Honor of Manuel Berberian's Forty-Five Years
537 of Research Contributions: Geological Society of America Special Paper 525, p. 1–84,
538 doi:10.1130/2016.2525(04)

539 Berberian, M., Qorashi, M., Arzhangravesh, B., and Mohajer-Ashjai, A., 1985. Recent Tectonics, Seismotectonics
540 and Earthquake-Fault Hazard Study in the Greater Tehran Region: Geological Survey of Iran, Report no.
541 56, 130 p. [in Persian].

542 Bufe, A., Burbank, D.W., Liu, L., Bookhagen, B., Qin, J., Chen, J., Li, T., Thompson Jobe, J.A., and Yang, H.,
543 2017. Variations of lateral bedrock erosion rates control planation of uplifting folds in the foreland of the
544 Tian Shan, NW China. Journal of Geophysical Research: Earth Surface, 122, 2431–2467.
545 https://doi.org/10.1002/2016JF004099

546 Buylaert, J.P., Murray, A.S., Thomsen, K.J., Jain, M., 2009. Testing the potential of an elevated temperature IRSL
547 signal from K-feldspar. Radiation Measurements 44, 560–565.
548 https://doi.org/10.1016/j.radmeas.2009.02.007

549 Coward, M.P., 1994. Inversion tectonics. In Continental Deformation. Edited by P.L. Hancock. Pergamon Press.
550 280-304.

551 Dahlstrom, C.D.A., 1970. Structural geology in the eastern margin of the Canadian Rocky Mountains. Canad.
552 Petrol. Geol. Bull., 18, 332-406.

553 DeCelles, P.G., Giles, K.A., 1996. Foreland basin systems. Basin Research 8, 105-123.

https://doi.org/10.5194/egusphere-2025-500
Preprint. Discussion started: 1 July 2025

Djamour, Y., Vernant, P., Bayer, R., Nankali, H. R., Ritz, J.-F., Hinderer, J., Hatam, Y., Luck, B., Le Moigne, N., Sedighi, M., and Khorrami, F., 2010. GPS and gravity constraints on continental deformation in the Alborz mountain range, Iran: GPS and gravity measurements in Alborz, Geophysical Journal International, 183, 1287–1301, https://doi.org/10.1111/j.1365-246X.2010.04811.x

Duller, G.A.T., 2007. Assessing the error on equivalent dose estimates derived from single aliquot regenerative dose measurements 25, 10.

Durcan, J.A., King, G.E., Duller, G.A.T., 2015. DRAC: Dose Rate and Age Calculator for trapped charge dating. Quaternary Geochronology 28, 54–61. https://doi.org/10.1016/j.quageo.2015.03.012

Gans, C.R., and Furlong, K.P., 2003. Fault creep and microseismicity on the Hayward fault, California: Implications for asperity size. Geophysical Research Letters, 30(19), 2000, doi:10.1029/2003GL017904.

Florensov, N.A., and Solonenko, V.P. (eds), 1963. The Gobi-Altai earthquake. Moscow, Akademiya Nauk USSR [in Russian] [English translation by Israel Program for Scientific Translations] 1965, Department of Commerce Washington, DC, US.

Ghassemi, M.R., 2016. Surface ruptures of the Iranian earthquakes 1900–2014: Insights for earthquake fault rupture hazards and empirical relationships. Earth Science Reviews, 156, 1-13.

Ghassemi, M.R., 2023. Inheritance of geology and geomorphology amidst urban growth: Historical development of the Tehran Metropolitan area, Iran. Geoheritage, 15:119. https://doi.org/10.1007/s12371-023-00882-1

Ghassemi, M.R., Allen, M.B., and Motamedi, H., 2023. A synthesis of the geology and petroleum geology of the Iranian portion of the South Caspian Basin and surrounding areas. Journal of Petroleum Geology, 46(4), 487-512.

Guérin, G., Mercier, N., 2012. Preliminary insight into dose deposition processes in sedimentary media on a scale of single grains: Monte Carlo modelling of the effect of water on the gamma dose rate. Radiation Measurements 47, 541–547. https://doi.org/10.1016/j.radmeas.2012.05.004

Guérin, G., Mercier, N., Adamiec, G., 2011. Dose-rate conversion factors: update. Ancient TL 29, 5–8.

Heydari, M., and Ghassemi, M.R., 2025. Revisiting the dip-slip rate of the North Tehran Fault (Northern Iran) through studying the faulted materials and geomorphic markers. Tectonophysics, 897 (2025) 230610. https://doi.org/10.1016/j.tecto.2024.230610.

Heydari, M., Ghassemi, M.R., Grützner, C., Tsukamoto, S., Chruścińska, A., Preusser, F., 2024. First luminescence dating of exhumed fault-zone rocks of the North Tehran Fault (Iran). Quaternary Geochronology 101562. https://doi.org/10.1016/j.quageo.2024.101562

Heydari, M., Guérin, G., Sirakov, N., Fernandez, P., Ferrier, C., Guadelli, A., Leblanc, J.-C., Taneva, S., Sirakova, S., Guadelli, J.-L., 2022. The last 30,000 to 700,000 years ago: Unravelling the timing of human settlement for the Palaeolithic site of Kozarnika. Quaternary Science Reviews 291, 107645. https://doi.org/10.1016/j.quascirev.2022.107645

https://doi.org/10.5194/egusphere-2025-500
Preprint. Discussion started: 1 July 2025

Heydari, M., Guérin, G., Kreutzer, S., Jamet, G., Kharazian, M.A., Hashemi, M., Nasab, H.V., Berillon, G., 2020. Do Bayesian methods lead to more precise chronologies? 'BayLum' and a first OSL-based chronology for the Palaeolithic open-air site of Mirak (Iran). Quaternary Geochronology 59, 101082. https://doi.org/10.1016/j.quageo.2020.101082

Heydari, M., Guérin, G., 2018. OSL signal saturation and dose rate variability: Investigating the behaviour of different statistical models. Radiation Measurements 120, 96–103. https://doi.org/10.1016/j.radmeas.2018.05.005

Huntley, D.I., Baril, M., 1997. The K content of the K-feldspars being measured in optical dating or in thermoluminescence dating. Ancient TL 15, 11–13.

Huntley, D.J., Godfrey-Smith, D.I., Thewalt, M.L.W., 1985. Optical dating of sediments. Nature 313, 105e107.

Iaffa, D.N., Sàbat, F., Muñoz, J.A., Mon, R., and Guterrez, A.A., 2011. The role of inherited structures in a foreland basin evolution. The Metán Basin in NW Argentina. Journal of Structural Geology, 33 (2011) 1816-1828.

Jordan, T.E., Isacks, B.L., Allmendinger, R.W., Brewer, J.A., Ramos, V.A., Ando, C.J., 1983. Andean tectonics related to geometry of subducted Nazca plate. GSA Bulletin 94, 341-361.

Khorrami, F., Vernant, P., Masson, F., Nilfouroushan, F., Mousavi, Z., Nankali, H., Saadat, S.A., Walpersdorf, A., Hosseini, S., Tavakoli, P., Aghamohammadi, A., and Alijanzade, M., 2019. An up-to-date crustal deformation map of Iran using integrated campaign-mode and permanent GPS velocities, Geophysical Journal International, 217, 832–843, https://doi.org/10.1093/gji/ggz045

Kreutzer, S., Burow, C., Dietze, M., Fuchs, M.C., Schmidt, C., Fischer, M., Friedrich, J., Mercier, N., Philippe, A., Riedesel, S., Autzen, M., Mittelstrass, D., Gray, H.J., Galharret, J.-M., 2023. Luminescence: Comprehensive Luminescence Dating Data Analysis (v0.9.21). CRAN. https://doi.org/10.5281/zenodo.596252

Kreutzer, S., Schmidt, C., DeWitt, R., Fuchs, M., 2014. The a-value of polymineral fine grain samples measured with the post-IR IRSL protocol. Radiation Measurements 69, 18–29. https://doi.org/10.1016/j.radmeas.2014.04.027

Kreutzer, S., Schmidt, C., Fuchs, Margret, Dietze, M., Fischer, M., Fuchs, Markus, 2012. Introducing an R package for luminescence dating analysis. Ancient TL 30, 1–8.

Lin, S., and Williams, P.F., 1992. Ridge-in-groove slickenside striae in S-C mylonite. J. Struct. Geol. 14, 315-321.

Mattei, M., Cifelli, F., Alimohammadian, H., Rashid, H., Winkler, A., Sagnotti, L., 2017. Oroclinal bending in the Alborz Mountains (Northern Iran): New constraints on the age of South Caspian subduction and extrusion tectonics. Gondwana Research, 42, 13-28. https://doi.org/10.1016/j.gr.2016.10.003.

McMechan, M.E., 2023. Structural geometry and kinematic evolution of the central Canadian Rocky Mountain Foothills fold-and-thrust belt: Complex kinematic relationships controlled by detachment utilization. Geosphere, 19(6), 1690-1708. https://doi .org /10.1130 /GES02623.1.

Nelson, M.S., Rittenour, T.M., 2015. Using grain-size characteristics to model soil water content: Application to dose-rate calculation for luminescence dating. Radiation Measurements 81, 142–149. https://doi.org/10.1016/j.radmeas.2015.02.016

https://doi.org/10.5194/egusphere-2025-500
Preprint. Discussion started: 1 July 2025

Prescott, J.R., Hutton, J.T., 1994. Cosmic ray contributions to dose rates for luminescence and ESR dating: Large depths and long-term time variations. Radiation Measurements 23, 497–500. https://doi.org/10.1016/1350-4487(94)90086-8

Prescott, J.R., Stephan, L.G., 1982. The contribution of cosmic radiation to the environmental dose for thermoluminescence dating. Latitude, altitude and depth dependences. Journal of the European Study Group on Physical, Chemical and Mathematical Techniques Applied to Archaeology (PACT) 17–25.

Preusser, F., Degering, D., Fuchs, M., Hilgers, A., Kadereit, A., Klasen, N., Krbetschek, M., Richter, D., Spencer, J.Q.G., 2008. Luminescence dating: basics, methods and applications. E&G Quaternary Sci. J. 57, 95–149. https://doi.org/10.3285/eg.57.1-2.5

R Core Team, 2023. R: A Language and Environment for Statistical Computing.

Rieben, E.H., 1955. The geology of Tehran plain. Am. J. Sci., 253, 617–639.

Rieben, E.H., 1966. Geological observations on alluvial deposits in northern Iran. Geological Survey of Iran, Report No. 9. 39 p.

Ritz, J.-F., Nazari, H., Balescu, S., Lamothe, M., Salamati, R., Ghassemi, A., Shafei, A., Ghorashi, M., and Saidi, A., 2012. Paleoearthquakes of the past 30,000 years along the North Tehran Fault (Iran), J. geophys. Res., 117(B6), doi:10.1029/2012JB009147.

Rosas, F.M., Duarte, J.C., Almeida, P., Schellart, W.P., Riel, N., and Terrinha, P., 2017. Analogue modelling of thrust systems: Passive vs. active hanging wall strain accommodation and sharp vs. smooth fault-ramp geometries, Journal of Structural Geology, 99, 45-69.

Schwanghart, W., and Scherler, D., 2014. Short Communication: TopoToolbox 2 – MATLAB-based software for topographic analysis and modeling in Earth surface sciences. Earth Surface Dynamics, 2(1), 1–7. Copernicus GmbH. Retrieved from https://doi.org/10.5194%2Fesurf-2-1-2014

Solaymani-Azad, S., 2023. Active seismogenic faulting in the Tehran Region, north of Iran; state-of-the-art and future seismic hazard assessment prospects. Tectonophysics, 856, 229843. https://doi.org/10.1016/j.tecto.2023.229843

Strabo, ed. & trans. H.L. Jones. 1969. The geography of Strabo, Loeb Classical library, London.

Talebian M., Copley, A.C., Fattahi, M., Ghorashi, M., Jackson, J.A., Nazari, H., Sloan, R.A., and Walker, R.T., 2016. Active faulting within a megacity: the geometry and slip rate of the Pardisan thrust in central Tehran, Iran. Geophysical Journal International, 207, 1688–1699.

Vernant, P., Nilforoushan, F., Chery, J., Bayer, R., Djamour, Y., Masson, F., Nankali, H., Ritz, J.-F., Sedighi, M., and Tavakoli, F., 2004. Deciphering oblique shortening of central Alborz in Iran using geodetic data, Earth and Planetary Science Letters, 223, 177–185. https://doi.org/10.1016/j.epsl.2004.04.017

von Hagke, C., Bauville, A., and Chudalla, N., 2024. Control of décollement strength and dip on fault vergence in fold-thrust belts and accretionary prisms. Tectonophysics, 870, 230172.

https://doi.org/10.5194/egusphere-2025-500
Preprint. Discussion started: 1 July 2025

659 Wells, D.L., and Coppersmith, K.J., 1994. New Empirical Relationships among Magnitude, Rupture Length,
660 Rupture Width, Rupture Area and Surface Displacement, Bulletin of the Seismological Society of America,
661 84(4), 974-1002.

662 Yaminifard, F., Moradi, A., and Naghavi, M., 2012. Source parameters of the October 17, 2009 Rey-Tehran
663 earthquake, Mw 4.3. Iranian Journal of Geophysics, 6(3), 46-58.

664 Zhang, J., Li, S.H., 2020. Review of the post-IR IRSL dating protocols of K-feldspar. Methods Protocol 3, 7.